Power Engineering and Engineering Thermophysics
https://www.acadlore.com/journals/PEET

Progress in High-Entropy Alloy Performance Enhancement

Xinsheng Wang[1*], Jifeng Luo[1], Rongbin Ma[2], Kai Wang[3]

[1] School of Mechanical and Electrical Engineering, Zhengzhou University of Light Industry, Henan Key Laboratory of Intelligent Manufacturing of Mechanical Equipment, 430002 Zhengzhou, China
[2] School of Chemical Engineering and Materials Science, Xuchang University, 461002 Xuchang, China
[3] Zhengzhou Lijia Thermal Spraying Machinery Co., Ltd., 450000 Zhengzhou, China

[*] Correspondence: Xinsheng Wang (wangxs@zzuli.edu.cn)

Received: 12-07-2023 **Revised:** 01-24-2024 **Accepted:** 01-30-2024

Citation: X. S. Wang, J. F. Luo, R. B. Ma, and K. Wang, "Progress in high-entropy alloy performance enhancement," *Power Eng. Eng. Thermophys.*, vol. 3, no. 1, pp. 12–26, 2024. https://doi.org/10.56578/peet030102.

Abstract: High-entropy alloy (HEA) is currently regarded as materials with the most superior comprehensive properties, possessing capabilities not found in traditional alloys. This is particularly attributed to the characteristic presence of multiple principal elements, endowing the alloys with exceptional performance across various aspects, thus becoming a focal point of both current and future research endeavors. The performance of HEA is derived from phase transition. This review summarizes the intrinsic phase transition of HEA itself and the enhancement of HEA performance through the addition of particulate phases. Starting from the definition of HEA, the common definitions are introduced, leading to the design principles of HEA and the prediction of solid solution phases. The influence of different elements on the structural changes of HEA solid solution phases is explained through lattice distortion phase transition and segregation phase transition methods. The patterns of phase transition induced by large atomic elements are summarized, and the development process of segregation phase transition by small atomic elements is presented, offering references for future research on HEA. Furthermore, the concept of solubility of elements in HEA is introduced, based on the phase transition caused by large and small atomic elements, providing a more accurate basis for the design and preparation of HEA. The common hard particles used to enhance the performance of HEA are discussed, revealing how direct addition of particles can lead to decomposition and the uncertainty of the effects of elements on HEA performance. The significance of encapsulation techniques in enhancing the performance of high-quality HEA is proposed.

Keywords: High-entropy alloy; Laser cladding; Phase transition; Distortion; Segregation

1 Introduction

Traditional alloy materials are predominantly composed of iron, cobalt, nickel, titanium, and similar metals [1–4]. The practice of enhancing alloy performance by adding a small amount of other elements to one or two principal elements, although superior to coatings made from a single metal, is not without its challenges. Research has shown that intermetallic compounds, which can form between different metals, are prevalent in these alloys, leading to a multitude of complex intermetallic compounds. Greer [5] defined this phenomenon as the confusion principle. Furthermore, according to Gibbs' phase rule, the presence of n elements in an alloy, whether in equilibrium or not, will result in at least n+1 compound phases, with an increase in compound phases inevitably leading to a deterioration in alloy performance [6, 7]. The introduction of the confusion principle and the calculations based on Gibbs' phase rule brought research on alloy elements to a standstill until Yeh et al. [8] and Cantor et al. [9] proposed the concept of HEA. HEA, characterized by its composition of five or more elements in equiatomic ratios, represents a novel alloy theory. Predominantly featuring a solid solution structure, HEA breaks away from the chaos of intermetallic compounds. The concurrent presence of multiple principal elements enhances the coating's strength, hardness, and corrosion resistance [10–12].

1.1 Definition of HEA

Currently, the definition of HEA is categorized into three types: definitions based on atomic ratio, entropy value, and phase. The definition based on atomic ratio, proposed by Professor Ye Junwei, categorizes the alloy containing

five or more elements, with each element's atomic ratio ranging from 5% to 35%, as HEA. This initial definition merely outlines the element proportion and has been expanded upon with increased usage and research on HEA, with the requirements for the atomic ratios of elements not strictly limited to within 5% to 35%.

The definition based on entropy value stems from Boltzmann's hypothesis, introducing the concept of entropy $\Delta \mathrm{S_{mix}}$ into the alloy. The calculation is shown in Eq. (1) [13], where R represents the Boltzmann gas constant, valued at $8.31\ \mathrm{J/\left(k^{*}\ mol\right)}$, n is the number of principal elements in the alloy, and C_i is the atomic percentage of the i-th element in the alloy system.

$$\Delta \mathrm{S_{mix}} = -\mathrm{R}\sum_{\mathrm{i}=1}^{\mathrm{n}}\left(\mathrm{C_i}\ln C_i\right) \tag{1}$$

When the entropy exceeds $1.5\mathrm{R}$, the alloy system tends to form a disordered arrangement of solid solution structures rather than complex intermetallic compounds [14]. The entropy of HEA is directly proportional to the number of principal elements; the higher the entropy, the more inclined the system is to form solid solution structures. The alloy is classified based on its entropy value into HEA ($\triangle\ \mathrm{S_{mix}} \geq 1.5R$), medium-entropy alloy ($1R \leq \triangle \mathrm{S_{mix}} < 1.5R$), and low-entropy alloy ($\triangle \mathrm{S_{mix}} < 1R$). However, studies have found that when the number of principal elements reaches thirteen, the impact of additional elements on the properties of HEA becomes increasingly negligible. Thus, the number of principal elements in HEA is controlled to be between five and thirteen [15].

Designing HEA solely based on the concepts of entropy and atomic ratio has proven insufficient for the successful synthesis of HEA. For instance, Xian's attempt to fabricate VTiFeCrZr HEA, adhering to the atomic ratio concept with each element's atomic ratio meeting the 5% to 35% criterion (entropy $\Delta \mathrm{S_{mix}} \approx 1.6\mathrm{R}$) and the entropy aligning with the concept of HEA, should theoretically result in the formation of HEA. However, the alloy experienced brittleness and fracturing after synthesis, failing to become HEA with superior properties [16].

Currently, the most accurate approach to determining HEA is through phase determination. The emergence of HEA is mainly attributed to the mixture of multiple elements not resulting in a multitude of intermetallic compound phases as predicted by the confusion principle, which would lead to alloy brittleness. Instead, there is a tendency to form solid solution structures. Therefore, it is commonly accepted that any alloy composed of five or more elements that can form a solid solution structure may be classified as a HEA, thus relaxing the requirements for atomic ratio and entropy value. However, the formation of a solid solution structure remains a stringent condition for HEA, prompting numerous researchers to investigate design principles for HEA to successfully achieve the required solid solution structure.

2 Design Basis of HEA

The current basis for HEA design is divided into three categories: atomic radius difference δ and mixing enthalpy ΔH_{mix}, atomic radius difference δ and entropy enthalpy Ω, and the improved atomic radius difference γ.

2.1 Design Basis of Atomic Radius Difference and Mixing Enthalpy

Zhang et al. [17] inferred two criteria for the formation of solid solutions in HEA using the HumeRothery rules: the difference in atomic radius (δ) and mixing enthalpy $(\triangle H_{mix})$.

In HEA, the traditional distinction between solute and solvent does not apply, as each element serves as both solute and solvent for the others. A significant difference in atomic radius can exacerbate lattice distortion, increase strain energy, and raise the alloy's free energy, leading to reduced stability of the solid solution. Additionally, the difference in atomic radius can slow down diffusion rates, reduce the rate of phase transition, and lead to segregation of atoms within the alloy. Therefore, the impact of atomic size must be considered in the design of HEA, where the atomic radii should be maintained at similar levels. The formula for calculating atomic radius difference is shown in Eq. (2) [17].

$$\delta = \sqrt{\sum_{\mathrm{i}=1}^{\mathrm{n}}\mathrm{C_i}\left(1-\frac{\mathrm{r_i}}{\bar{\mathrm{r}}}\right)^2} \tag{2}$$

where, C_i is the atomic percentage of the i-th element, r_i is the atomic radius of the i-th element, and $\bar{r}$ is the average atomic radius of $\sum_{i=1}^{n} C_i r_i$.

Enthalpy $\triangle H_{\mathrm{mix}}$ indicates the strength of the atomic bonds. In HEA, the closer $\triangle H_{\mathrm{mix}}$ is to zero, the easier it is to form a solid solution without causing segregation or forming intermetallic compounds. The calculation formula for ΔH_{mix} is shown in Eq. (4) [18].

$$\Delta \mathrm{H_{mix}} = \sum_{\mathrm{i=1,j\neq i}}^{\mathrm{n}} \Omega_{\mathrm{ij}} \mathrm{C_i C_j} \tag{3}$$

$$\Omega_{\mathrm{ij}} = 4\Delta \mathrm{H_{AB}^{mix}} \tag{4}$$

$\triangle H_{AB}^{\mathrm{mix}}$ can be found in the study of Takeuchi and Inoue [19]. In Zhang et al. [17]'s criteria for forming stable solid solutions, as illustrated in Figure 1, alloys tend to form stable solid solution structures when the atomic radius difference $\delta \leq 6.6\%$ and mixing enthalpy $-20 \leq \triangle \mathrm{H_{mix}} \leq 5\mathrm{kj/mol}$.

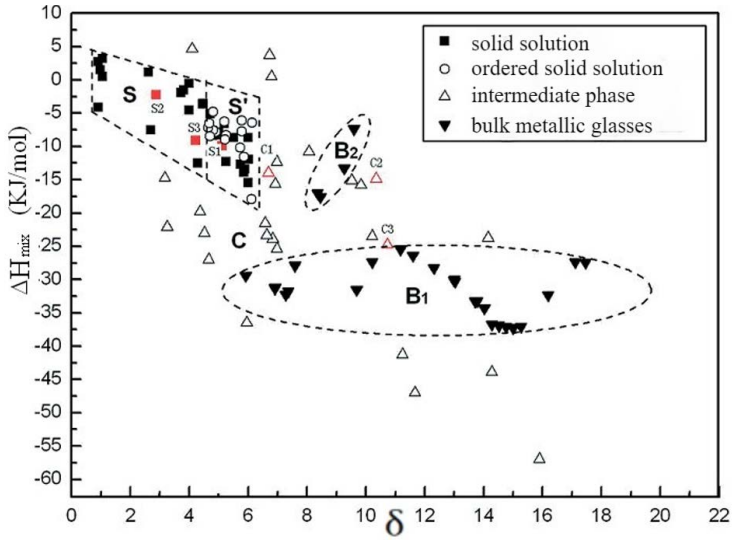

Figure 1. Relationship between $\delta, \triangle H_{AB}^{mix}$ and HEA phase [17]

2.2 Design Basis of Atomic Radius Difference and Entropy-Enthalpy

Mixing enthalpy is used to calculate the state of disorder in HEA, with a larger magnitude of $|\triangle H_{\mathrm{mix}}|$ indicating greater disorder and a lower likelihood of forming a solid solution structure [20, 21]. Entropy $\triangle S_{\mathrm{mix}}$ plays a role in inhibiting the formation of intermetallic compounds in HEA; the greater the entropy, the more stable the HEA. Given the simultaneous presence of entropy and enthalpy in HEA, it is insufficient to consider mixing enthalpy alone as the basis for forming solid solution structures; both entropy and enthalpy should be taken into account. Hence, Yang and Zhang [22] proposed the entropy-enthalpy basis, suggesting that entropy and enthalpy exhibit a competing relationship in HEA. If entropy exceeds enthalpy, the formation of a solid solution is favored; if enthalpy exceeds entropy, segregation or an increase in intermetallic compounds occurs, hindering the formation of solid solution structures, as indicated in Eqs. (5) and (6) [22].

$$\Omega = \frac{T_m \Delta S_{mix}}{|\Delta H_{mix}|} \tag{5}$$

$$T_m = \sum_{i=1}^{n} C_i \left(T_m\right)_i \tag{6}$$

where, $\left(T_m\right)_i$ represents the melting point of the i-th alloy.

Yang and Zhang [22] established a relationship diagram between δ and Ω through extensive data, as shown in Figure 2. From this diagram, one can intuitively understand the effects of δ and Ω on HEA. The S region indicates the presence of only solid solutions, the I region indicates only intermetallic compounds, the S+I region indicates the coexistence of solid solutions and intermetallic compounds, and the B region is where amorphous phases form. Analysis reveals that to form a solid solution phase in HEA, specific criteria must be met, i.e., $\Omega \geq 1.1$, and $\delta \leq 6.6\%$.

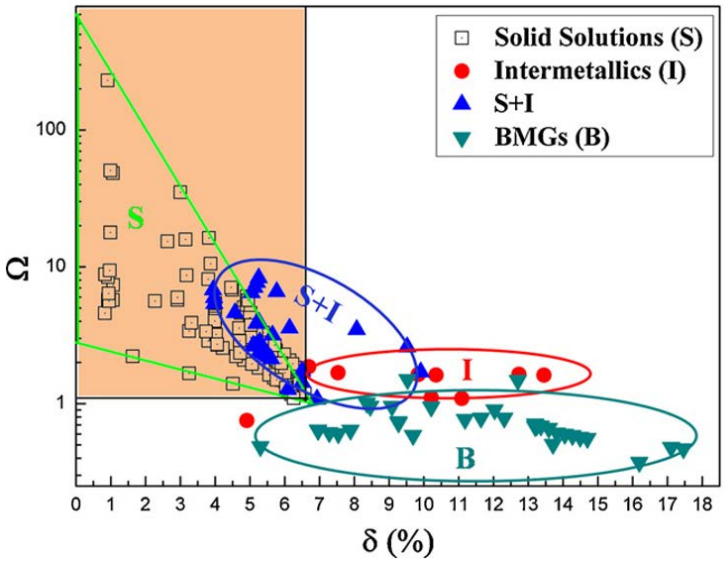

Figure 2. Relationship between δ, Ω and phase structure of HEA [22]

2.3 Design Basis of Improved Atomic Radius Difference

Yang and Zhang [22] introduced the concept of simultaneous entropy-enthalpy influence for determining the formation of alloy solid solutions, without suggesting improvements to the atomic radius difference, considering it suitable. However, Guo et al.'s [23] research identified shortcomings in the formula for atomic radius difference for some HEA. As shown in Figure 3, $\delta \leq 6.6\%$, and $-20 \leq \triangle H_{mix} \leq 5\mathrm{kj/mol}$ proposed [23] are the blue shaded area in the diagram, which do not exclusively contain solid solution structures but also intermetallic compounds.

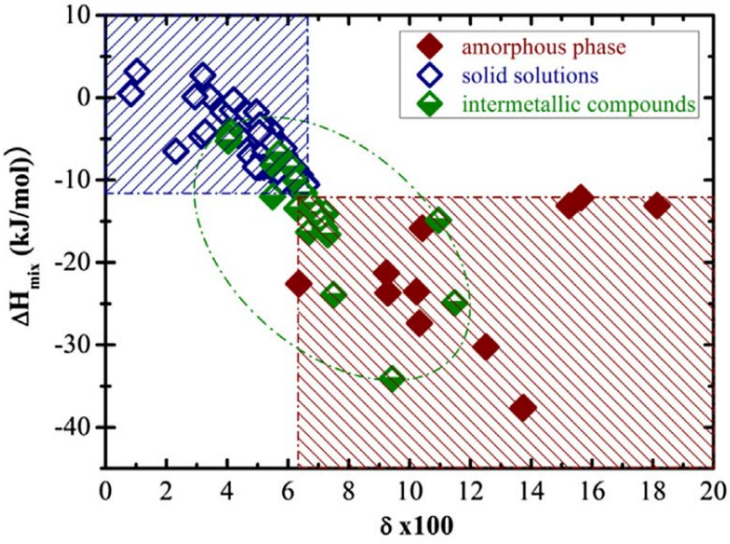

Figure 3. $\delta - \triangle H$ [23]

Addressing this phenomenon, Wang et al. [24] proposed a modification to the atomic radius difference criterion, as demonstrated in Eq. (7):

$$\gamma = \frac{1 - \sqrt{\frac{(\mathrm{r}_S + \bar{r})^2 - \bar{r}^2}{(\mathrm{r}_S + \bar{r})^2}}}{1 - \sqrt{\frac{(\mathrm{r}_L + \bar{r})^2 - \bar{r}^2}{(\mathrm{r}_L + \bar{r})^2}}} \tag{7}$$

where, r_s is the maximum atomic radius, and r_L is the minimum atomic radius.

The comparison between the new atomic radius criterion formula and the original atomic radius criterion formula is illustrated in Figure 4.

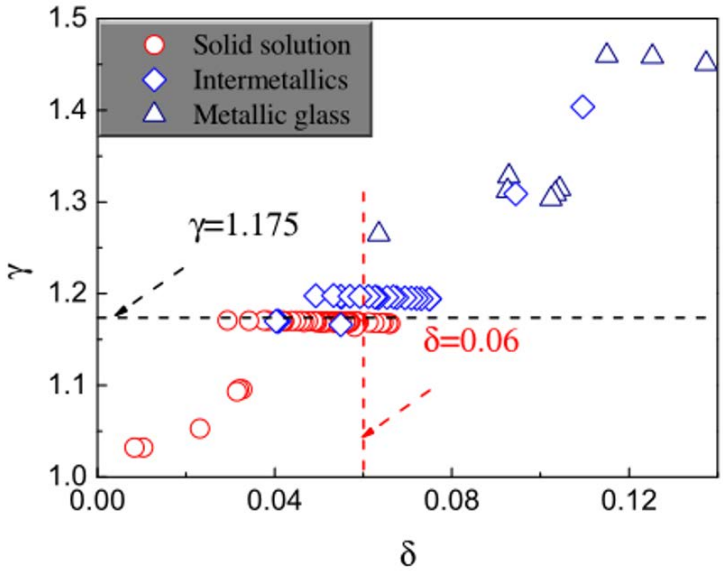

Figure 4. $\delta - \gamma$ phase division comparison diagram [24]

Analysis of the $\delta - \gamma$ diagram indicates that the division using $\gamma < 1.175$ is significantly more accurate and results in smaller errors compared to that using $\delta \leq 6.6\%$.

2.4 Prediction of HEA Phase Structure

Regardless of the criteria used, they only ensure the formation of a solid solution in HEA but do not determine the type of solid solution. For predicting the solid solution structure of HEA, Guo et al. [25] introduced the concept of valence electron concentration (VEC) to predict face-centered cubic lattice (FCC) and body-centered cubic lattice (BCC) phases.

The calculation of VEC proposed by Guo et al. [25] is shown in Eq. (8):

$$VEC = \sum_{i=1}^{n} C_i (VEC)_i \tag{8}$$

$(VEC)_i$ represents the VEC of element i. Through calculations and extensive experimental data, it has been determined that HEA tends to form FCC phases when $VEC \geq 8$, and BCC phases when $VEC < 6.87$. However, VEC is not suitable for predicting HEA containing Mn.

Table 1 presents the currently used data ranges for designing HEA to form solid solution structures and the basis for dividing HEA solid solution phases.

Table 1. Common solid solution basis and phase prediction

Solution Basis	$\delta \leq 6.6\%$ $-20 \leq \triangle H_{\text{mix}} \leq 5$ kj/mol	$\delta \leq 6.6\%$ $\Omega \geq 1.1$	$\gamma < 1.175$ $-20 \leq \triangle H_{\text{mix}} \leq 5$ kj/mol
Phase Prediction	VEC < 6.87 forms BCC phases, and $8 \leq$ VEC forms FCC phases		

3 Influence of Elements on HEA Phases

HEA is predominantly composed of solid solution phases. These solid solution phases are classified into three main types: FCC, BCC, and hexagonal close-packed structure (HCP). Research has indicated that in HEA, FCC and BCC phases constitute the majority of phase types; hence, studies primarily focus on these two phases.

The BCC phase, characterized by a body-centered cubic lattice, exhibits a structure where a cube encases a central atom, resulting in materials with higher hardness due to this configuration. Conversely, the FCC phase, featuring a face-centered cubic lattice, includes an atom embedded in each face of the cube, thereby providing more slip planes and directions, and consequently, better plasticity [26, 27].

To balance the toughness and hardness of HEA and enhance their overall performance, phase transition is often required. The elements that most significantly induce phase transition in HEA are categorized into two main

types: distortion phase transition and segregation phase transition. Distortion phase transition occurs with larger atomic radius elements, causing phase structure changes through lattice distortion driven by atomic compression. Segregation phase transition utilizes the concept of mixing enthalpy, adding elements with higher mixing enthalpy values with the alloy's elements to form new phases through segregation [28]. As shown in Table 2, common elements are listed with their atomic radii, VEC, and lattice structures.

Table 2. Radius, VEC and lattice structure of common elements [13, 29, 30]

Element	Symbol	Atomic No.	Radius $/\mathring{A}$	VEC	Lattice Structure
Aluminum	Al	13	1.432	3	-
Silicon	Si	14	1.153	4	-
Titanium	Ti	22	1.462	4	HCP
Chromium	Cr	24	1.249	6	BCC
Manganese	Mn	25	1.350	7	BCC
Iron	Fe	26	1.241	8	BCC/FCC
Cobalt	Co	27	1.251	9	HCP
Nickel	Ni	28	1.246	10	FCC
Copper	Cu	29	1.278	11	BCC

3.1 Distortion Phase Transition

It is generally considered that Al is a common element promoting the formation of BCC structures. In the $FeCoCrNiMnAl_x$ HEA, the structure remains a single-phase FCC solid solution when the Al content ranges from 0 to 8. With the addition of Al, the FCC phase gradually transition to the BCC phase, resulting in a dual-phase structure. When the content exceeds 16, a complete transition to the BCC phase structure occurs. In the dual-phase structure, the strength is higher than that of the single FCC phase, and the plasticity surpasses that of the single BCC phase [31]. In the lightweight $FeCrNiTi_{0.25}Al_x$, when $x > 0.5$, the HEA transition from an FCC+BCC phase to a dual BCC phase, one of which is the common disordered BCC phase found in HEA, and the other is an ordered BCC phase similar to NiAl. As shown in Figure 5, with the emergence of two BCC phases, the coating structure becomes denser, and the grains are progressively refined, with the two different BCC phases contributing to precipitation strengthening and nano-composite strengthening effects [32].

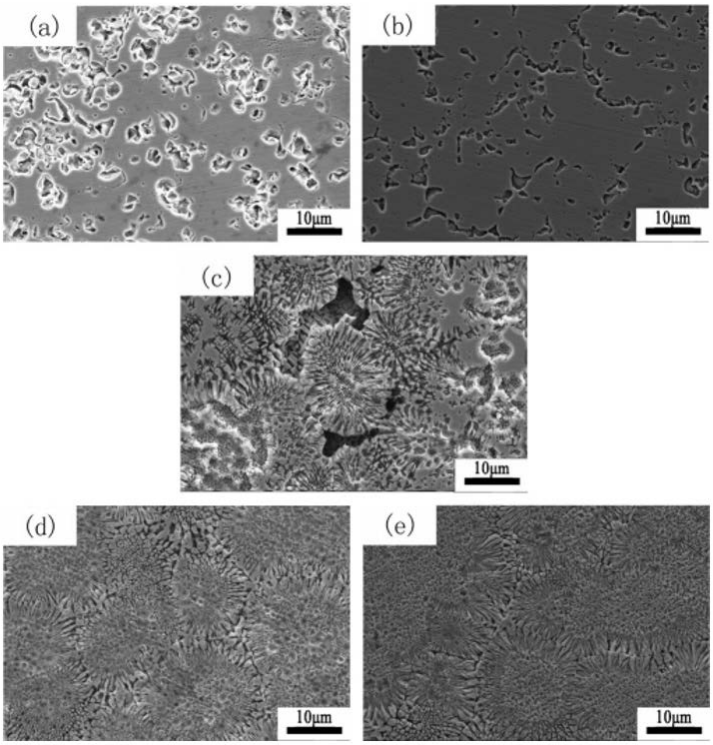

Figure 5. SEM pictures of $Al_xCrFeNiTiT_{0.25}$ alloys [32], (a) Al_0 (b) $Al_{0.25}$ (c) $Al_{0.5}$ (d) $Al_{0.75}$ (e) $Al_{1.0}$

The addition of Al is believed to facilitate the increase of the BCC phase primarily because the FCC phase has a higher structural density. When Al is added, lattice distortion occurs, energy increases, and the FCC phase becomes unstable, thus favoring the formation of the stable BCC phase to conserve energy [33].

In the phase transition diagram of $FeCoNiCrCuAl_x$ HEA shown in Figure 6, the presence of Ni and Al simultaneously, with Al content exceeding 0.5, invariably leads to the formation of an ordered Ni-Al BCC phase. When Al is further increased beyond its solubility in the BCC matrix, excess Al forms a rich-Al FCC phase [34–38].

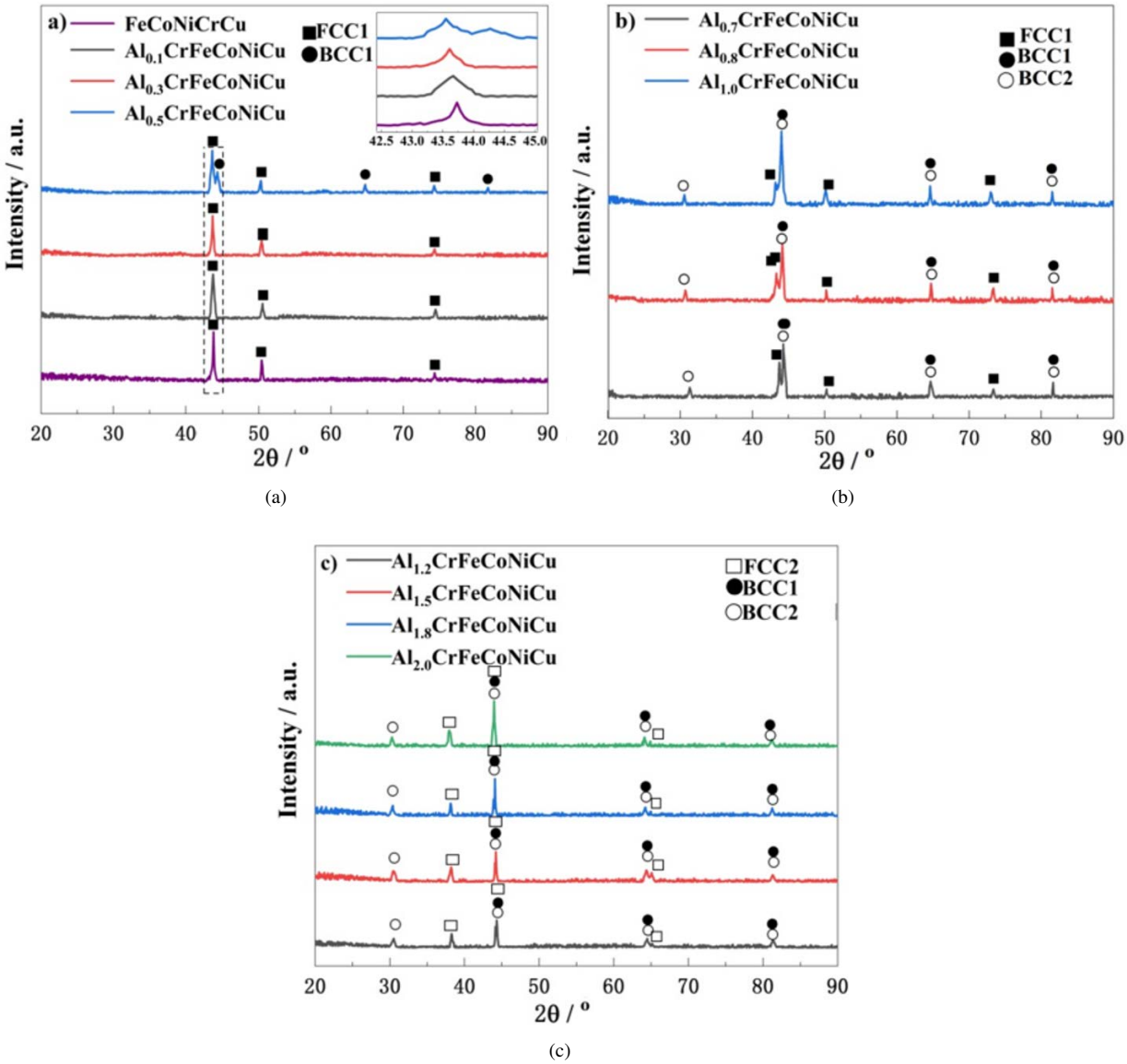

Figure 6. XRD spectra of $FeCoNiCrCuAl_x$ coatings (a) low-aluminum coatings (b) medium-aluminum coatings (c) high-aluminum coatings [34]

As indicated in Table 2, the atomic radius of Ti is larger than that of Al, increasing the likelihood of distortion phase transition. Research on the influence of Ti on HEA revealed that Ti promotes the formation of BCC structures. In the study of $AlCoCrFeNiTi_x$ HEA by Liu et al. [39], AlCoCrFeNi was solely a BCC phase without Ti. Upon reaching a Ti content of 0.4, a new BCC phase emerges, resulting in a dual-BCC phase structure [35]. However, Ti's ability to promote BCC formation was not observed in the FCC phase HEA of CoCrFeNiTi, with no BCC phase appearance even when x reached 0.7 in $CoCrFeNiTi_x$ [36]. Figure 7 illustrates the phase transition diagram in $CoCr_{2.5}FeNi_2Ti_x$ HEA with BCC phases, showing the BCC phase of HEA diminishing with the addition of Ti, the emergence of the FCC phase, and gradually becoming the dominant phase structure. At an addition level of 1.5, the FCC phase transition back to the BCC phase, making it the primary phase structure once more [37].

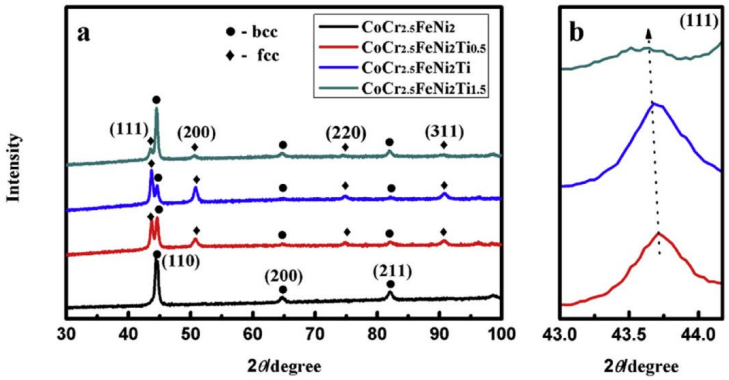

Figure 7. Phase transition diagram of with varying Ti content in HEA [37]

As indicated in Table 2 and Table 3 [38–46], the addition of large atomic elements to HEA follows a distinct phase transition pattern. When large atomic elements are added to HEA with an FCC phase, the FCC phase of the HEA transition to a structurally stable BCC phase as the amount of the element increases. Conversely, when large atomic elements are added to HEA with a structurally stable BCC phase, the large atomic elements first dissolve, filling the spaces within the BCC structure to form a dense FCC phase. With further increases in element content, the FCC phase, due to the increase in energy, again distorts into the BCC phase.

Table 3. Influence of elements on phase transition in HEA

HEA	Content	Phase	Reference
$FeCoCrNiMnAl_x$	< 8	FCC	[23]
	$8 \sim 16$	FCC + BCC	
	> 16	BCC	
$FeCrNiTi_{0.25}Al_x$	< 0.5	FCC + BCC	[24]
	> 0.5	BCC + BCC	
$FeCoNiCrCuAl_x$	< 0.5	FCC	[26]
	$0.5 \sim 1$	FCC + BCC	
	> 1	FCC + BCC + FCC1	
$CoCr_{2.5}FeNi_2Ti_x$	0	BCC	[35]
	0.5	BCC + FCC	
	1	BCC < FCC	
	1.5	BCC > FCC	
$FeNiCrCoSi_x$	0	FCC	[39, 40]
	0.5	BCC > FCC	
	2	BCC	
$MoFeCrTiWSi_x$	< 0.2	BCC	[41]
	> 0.4	BCC+Laves	
$AlCoCrFeNiMnCu_x$	< 0.6	BCC	[43]
	$0.6 \sim 0.8$	BCC + FCC1	
	0.8	BCC + FCC1 + FCC2	
$AlCoCrFeNiCu_x$	< 0.5	BCC	[44]
	$0.5 \sim 1$	BCC + FCC1	
	> 1	BCC + FCC1 + FCC2	
$CoCrFeNiCu_x$	$0 - 1$	FCC	[45, 46]

3.2 Segregation Phase Transition

Hedya et al. [35], while studying the impact of Si content on the properties of FeNiCrCo, discovered that CoCrFeNi presents an FCC phase structure. Upon the addition of Si to a concentration of 0.9, a small amount of BCC phase appears without significant changes to the FCC phase. As depicted in Figure 8, Hao et al. [36], extending previous research on Si addition, conducted further studies on phase transition in CoCrFeNi HEA. With increasing Si content, the FCC phase gradually diminishes, and the BCC phase becomes more prevalent, until at x=2, only the BCC phase exists, indicating that Si can transform the FCC phase into the BCC phase. Zhou et al. [37] investigated

the impact of Si on the properties of BCC phase structure HEA. In MoFeCrTiW with added Si, the primary structure of the HEA remains BCC. Due to the small mixing enthalpy between Si and other elements, which facilitates reaction, the addition of and more than 0.4 leads to the formation of intermetallic compounds. Although the MoFeCrTiWSi HEA is BCC, there is a significant presence of intermetallic compounds. However, the addition of Al reduces these compounds, implying that Al's introduction causes distortion in the HEA, increasing Si's solubility in the alloy, preventing the segregation-formed intermetallic compounds, and promoting the BCC phase's formation [41].

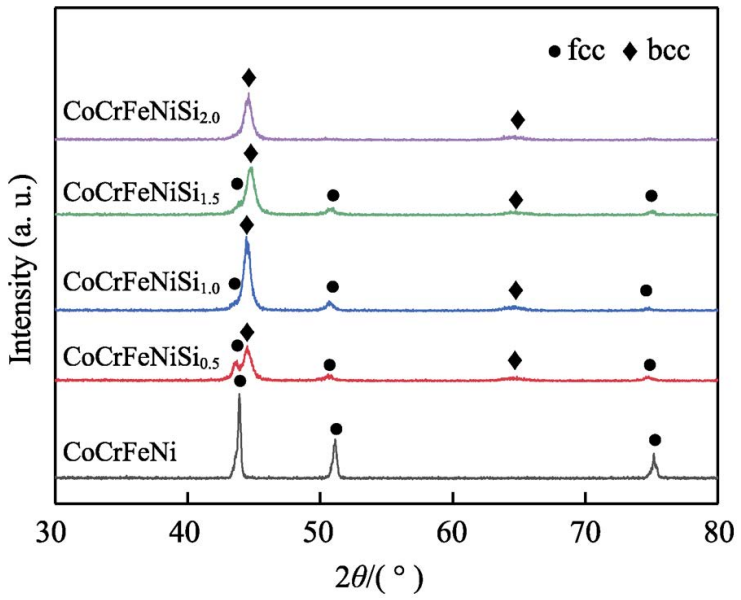

Figure 8. X-ray diffraction spectrum of $CoCrFeNiSi_x$ HEA coatings [39]

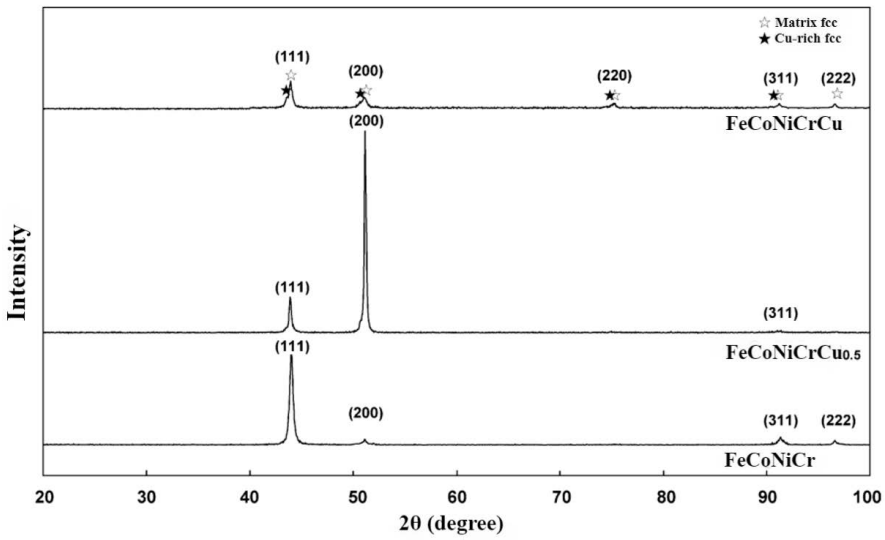

Figure 9. $CoCrFeNiCu_x$ phase analysis diagram [45]

Wu et al. [42], in studying the effect of Cu on AlCoCrFeNiMn HEA, found that as the Cu content increased, segregation intensified, transitioning from a single BCC phase to a dual BCC and FCC phase. Based on the calculation of mixing enthalpy, Cu has considerable difficulty dissolving with other elements. Therefore, when Cu content reaches 0.6, the alloy structure cannot dissolve Cu atoms, initiating segregation and expelling Cu to the grain boundaries to form a rich-Cu FCC phase. In the study of Zhu et al. [43] on the addition of Cu to AlCoCrFeNiCu HEA, when Cu content exceeded 0.5, the grain boundary became blurred, and the FCC phase appeared, similar to Wu et al.'s [42] findings. Initially, when the Cu content was low, it was entirely dissolved in the solid solution, hence the clear grain boundaries. However, as the content increased beyond the alloy's solubility limit for Cu, Cu segregated between dendrites, blurring the grain boundaries. When Cu content exceeded 1, the FCC phase became

predominant in the entire HEA structure. As shown in Figure 9, the addition of Cu to the CoCrFeNi single-phase FCC HEA, due to different solubility limits for Cu in the solid solution structure, led to two peaks in the HEA: one forming a Cu-rich FCC phase and the other a Cu-poor FCC phase [44, 45].

As demonstrated in Table 1 and Table 2, for small atomic elements like Si and Cu, adding significant amounts to the dense FCC phase can increase the distortion of the FCC phase, promoting the formation of the BCC phase. However, for HEA with a structurally stable BCC phase, these small atomic elements do not cause distortion; in such cases, the impact of mixing enthalpy is greater than the effect of solid solution distortion. Although the phase transition of small atomic elements primarily results from the segregation effect of mixing enthalpy, in HEA, even small atoms primarily dissolve before segregation occurs. This implies that there is a solubility between small atomic elements and HEA, and controlling this solubility is key to mastering segregation phase transition. From the perspective of phase transition of small atomic elements, the presence of intermetallic compounds is mostly due to the influence of mixing enthalpy; the smaller the mixing enthalpy among elements in HEA, the greater the likelihood of forming intermetallic compounds within the alloy.

In summary, phase transition caused by the lattice distortion of large atomic elements have a significant impact on the solid solution structure of the entire HEA, altering the overall phase structure type. In contrast, segregation phase transition by small atomic elements generally do not change the original structure type but segregate a portion of new phase structures near the grain boundaries, having a relatively minor impact on the overall structural performance of HEA.

4 Particle-Reinforced HEA

HEA is primarily composed of solid solution phases. A common misconception is that a solitary solid solution structure is the optimal structure; however, this is not necessarily the case. Although the presence of intermetallic compounds can lead to hardening of the alloy, this does not imply that the presence of intermetallic compounds is detrimental [46–48]. For instance, in the study of $\mathrm{Ni1.5CrCoFe0.5Mo0.1Nb_x}$ HEA by Peng et al. [49], it was found that with an increase in Nb, the coating transition from a single FCC phase to a mixture of FCC and Laves phases. The increase in Laves phases did not lead to embrittlement of the coating. On the contrary, it enhanced the hardness of the coating, transitioning from adhesive wear to abrasive wear, and improved the coating's wear resistance.

The introduction of elements to form intermetallic compounds within HEA can enhance the hardness and wear resistance, thus improving the overall performance of the alloy. However, this approach carries greater risks. The initial intention behind the design of HEA was to prevent the formation of intermetallic compounds and avoid brittle phases within the alloy. Therefore, adding hard particle phases to enhance the coating performance is a more prudent strategy.

The hardness enhancement of coatings with hard particles generally follows two paths: through their pinning effect, which inhibits grain growth, making the coating's microstructure denser and finer, and through the decomposition of particles within the coating, reacting with other elements in the alloy to form more hard phases. Hard particles that enhance the performance of HEA include WC, TiC, SiC, NbC, and $\mathrm{Al_2O_3}$. The properties of these particles are summarized in Table 4 [50–56]. Currently, WC and TiC are the most commonly applied particles in the field of HEA, with less research on other particles.

WC, known for its high hardness and melting point, is a commonly used particle reinforcement phase. The most extensively studied is the WC-reinforced FeCoCrNi series of HEA. Huang et al. [50] employed 20% WC to enhance the FeCoCrNi HEA. During the cladding process, a portion of the WC decomposed, resulting in the presence of FCC phase, WC phase, and $(\mathrm{Cr,W})_2\mathrm{C}$ compounds within the coating. Due to the presence of WC and $(\mathrm{Cr,W})_2\mathrm{C}$ hard phases, the hardness of FeCoCrNi was enhanced. Moreover, the disintegration of hard WC during wear transformed sliding dry friction into rolling friction, reducing the friction coefficient and enhancing the wear resistance of the coating. Zhang et al. [51] found that WC completely dissolved when enhancing FeCoCrNiCu, without any secondary phases emerging. Compared to FeCoCrNiCu, the BCC phase increased while the FCC phase decreased. WC dissolved entirely in the FCC, causing lattice distortion and promoting the transition from FCC to BCC phase. The solubility of WC also hindered grain growth, promoted grain refinement, and increased the coating's hardness. Adding WC can enhance the coating's hardness, but when the WC content exceeds 10%, the dilution rate of the coating increases, and the hardness decreases near the heat-affected zone.

Cai et al. [52] studied the enhancement effect of WC on FeCoCrNiB. Before adding WC, the coating structure exhibited a lamellar organization, consisting only of FCC and M3B phases. With the addition of 5% WC, the coating remained lamellar and M3C compound phases appeared. When WC content reached 10%, grains began to refine, and the lamellar organization transitioned to dendritic, significantly altering the phase structure. Carbide and boride compounds combined to form $\mathrm{M_{23}(C,B)_6}$ and $\mathrm{M_7(C,B)_3}$ phases. With further increase to $20\mathrm{wt\%}$ WC, all $\mathrm{M_7(C,B)_3}$ phases transformed into $\mathrm{M_{23}(C,B)_6}$ phases. With increasing WC content, the phase of the coating gradually transformed, and the hardness of the coating increased from $631\mathrm{HV}$ to $1159\mathrm{HV}$. At $20\mathrm{wt\%}$ WC content, the hardness reached its peak, and the wear volume was minimized.

Table 4. Performance statistics of particle-reinforced HEA

Particle	HEA	Content (wt %)	Vickers Hardness	Friction Weight Loss (mg)	Friction Coefficient	Reference
WC	FeCoCrNiCu	0	275			[50]
		10	501			
		20	634			
	FeCoCrNiB	0	631	4.2		[51]
		5	775	3.1		
		10	970	1.7		
		20	1159	0.8	0.4688	
TiC	FeCrNiCoMn	0	213.3	7.6	0.3688	[52]
		5	248.1	4.5	0.3415	
		10	266.4	4.2	0.4039	
		15	288.3	4.8		
NbC	FeCoCrNiAl	0	200	1.66	1.265	[54]
		10	384	1.31	1.258	
		20	525	1.05	1.023	
		30	458	1.17	1.034	
SiC	AlCoCrFeNi	0	200	1.66		[55]
		10	240	1.37		
		20	296	1.27		
		30	360	1.18		
Al_2O_3	AlCoCrFeNi	0	200	1.66	1.265	[56]
		10	475	1.27	1.148	
		20	426	1.32	1.345	
		30	459	1.31	1.307	

TiC, known for its high hardness and excellent high-temperature oxidation resistance, decomposes upon addition to coatings, forming carbides that enhance the coating's hardness. Additionally, during wear, Ti can oxidize to form TiO_2, which serves as a self-lubricating substance, reducing the coating's friction coefficient. Guo et al. [53] investigated the impact of TiC content on the wear resistance of FeCrNiCoMn HEA coatings. The study found that when the TiC content is below 5 wt%, the coating experiences both vertical and horizontal forces during friction. Due to the presence of hard phases, TiC particles bear the greatest force. With too few particles, each TiC particle undergoes significant stress, causing the TiC to break and thus decrease the coating's wear resistance. Conversely, when the TiC content is excessive, the adhesion between the coating and particles is insufficient, making the particles prone to being dislodged under stress. A 10 wt% TiC-enhanced coating significantly improves surface wear resistance but may suffer from fatigue wear, affecting the coating's wear life.

NbC is commonly used in the field of HEA, with Nb elements often added to HEA to promote the formation of hard Laves phases, enhancing the coating's hardness. Li et al. [54] employed NbC to reinforce the AlCoCrFeNi HEA coating. The addition of NbC promoted an increase in the BCC phase within the HEA while inhibiting the formation of the FCC phase. The introduction of NbC contributed to grain refinement and solid solution strengthening, leading to an initial increase followed by a decrease in the coating's hardness and wear resistance. With the addition of 20 wt% NbC particles, the coating's hardness peaked at 525HV, achieving optimal wear resistance.

Feng et al. [55] and Feng [56] utilized SiC and Al_2O_3 to enhance the performance of HEA, demonstrating that SiC, in laser-clad AlCoCrFeNi HEA, primarily contributes to solid solution strengthening and second phase strengthening, thereby increasing the coating's hardness. Moreover, the presence of SiC particles transforms adhesive wear into abrasive wear, reducing the coating's friction coefficient and enhancing its wear resistance. The addition of 10 wt% Al_2O_3 can improve the coating's hardness and wear resistance. However, excessive addition weakens the coating's performance, primarily due to the poor wettability between Al_2O_3 and the Q235 substrate material and the significant difference in thermal expansion coefficients. The inclusion of Al_2O_3 leads to defects such as porosity and cracks in the coating as it solidifies. When the amount of alumina added is low, alumina's solid solution strengthening and fine grain strengthening can enhance the coating's hardness and thereby its wear resistance. When added excessively, the increase in cracks and porosity defects causes a decline in performance.

There are two methods for adding particles: direct addition and in-situ synthesis. Direct addition is as introduced earlier. Although in-situ synthesis can offer better dispersion of particles compared to direct addition, it proves to

be an impractical technique for HEA. The principle of in-situ synthesis involves adding elements capable of forming corresponding hard phases into the cladding powder, where they react within the cladding layer to produce hard phases. However, given the multi-principal element nature of HEA, achieving the desired outcome through in-situ synthesis is challenging. The addition of elements for in-situ synthesis in HEA likely becomes a factor influencing phase transition, hence the limited application of in-situ synthesis techniques in the field of HEA.

Particle reinforcement technology and HEA constitute an optimal combination. HEA, devoid of other secondary phases, allows added particles to disperse without interference from other phases, resulting in more uniform distribution within the coating. This not only provides solid solution strengthening but also hinders grain growth, contributing to grain refinement. Especially, the combination of HEA with an FCC solid solution structure and hard particles is akin to incorporating hard particles into a soft matrix. The good plasticity of the matrix can achieve high bonding strength with hard particles, distributing them throughout the soft matrix to enhance the coating's hardness and wear resistance.

5 Conclusion

HEA is among the most superior performance alloys in the alloy field today, also exhibiting the cocktail effect, indicating that HEA has a long journey ahead with significant development potential. Future development of HEA could focus on the following two aspects:

(a) Refinement of elemental solubility in various HEA structures

Although there are many bases for the design of solid solutions in HEA, which have matured, regions that cannot be completely differentiated still exist in phase diagrams. Coupled with the cocktail effect of HEA, the future alloy elements will not be limited to five or six types of synthesis but will be a collection of more elements. Today's design bases become very complex for future design. The essence of HEA is to serve as a matrix carrying more elements without reacting. Whether it's distortion phase transition or segregation phase transition, solid solution remains the initial step. Therefore, a modular design approach could be adopted, using a solid solution of approximately five elements as the basis, to statistically determine the maximum solubility that can be added to the solid solution without causing phase transition. This approach could avoid extensive design calculations and maximize the use of the cocktail effect of HEA to enhance their performance by adding more elements.

(b) Particle-encapsulated enhancement of HEA

There are still some issues with particle-reinforced HEA. The elements decomposed from heated particles may form intermetallic compounds with elements within the HEA, affecting their performance. Future research could lean towards the study of particle-encapsulated enhancement of HEA to reduce particle decomposition. This not only adds hard phases but also prevents decomposed elements from forming brittle phases with elements within the HEA. The presence of multiple hard phases significantly improves the coating's hardness. By using particle encapsulation, decomposition is avoided, and more hard phases are not formed. Therefore, to further enhance the coating's hardness, different types of encapsulated particles can be added to the same coating to strengthen the coating's hardness.

Data Availability

The data used to support the findings of this study are available from the corresponding author upon request.

Conflicts of Interest

The authors declare no conflict of interest.

References

[1] M. Schinhammer, A. C. Hänzi, J. F. Löffler, and P. J. Uggowitzer, "Design strategy for biodegradable Fe-based alloys for medical applications," *Acta Biomater.*, vol. 6, no. 5, pp. 1705–1713, 2010. https://doi.org/10.1016/j.actbio.2009.07.039

[2] L. Wang, J. Mao, C. Xue, H. Ge, G. Dong, Q. Zhang, and J. Yao, "Cavitation-erosion behavior of laser cladded low-carbon cobalt-based alloys on 17-4PH stainless steel," *Opt. Laser Technol.*, vol. 158, p. 108761, 2023. https://doi.org/10.1016/j.optlastec.2022.108761

[3] R. Lachhab, M. Rekik, H. Azzeddine, T. Baudin, A. Helbert, F. Brisset, and M. Khitouni, "Study of the microstructure and texture heterogeneities of Fe–48wt% Ni alloy severely deformed by equal channel angular pressing," *J. Mater. Sci.*, vol. 54, no. 5, pp. 4354–4365, 2019. https://doi.org/10.1007/s10853-018-3114-6

[4] M. Geetha, A. Singh, R. Asokamani, and A. Gogia, "Ti based biomaterials, the ultimate choice for orthopaedic implants–A review," *Prog. Mater. Sci.*, vol. 54, no. 3, pp. 397–425, 2009. https://doi.org/10.1016/j.pmatsci.2008.06.004

[5] A. L. Greer, "Confusion by design," *Nature*, vol. 366, no. 6453, pp. 303–304, 1993. https://doi.org/10.1038/366303a0

[6] G. Wang, X. Li, and S. Wang, "Research progress of various high-entropy alloys," *J. Funct. Mater.*, vol. 50, no. 12, pp. 12 035–12 040, 2019.

[7] Y. Liu, Y. Li, X. Chen, and M. Chen, "Research progress in multi-principal element high entropy alloys," *Mater. Rev.*, vol. 2006, no. 4, 2006.

[8] J. W. Yeh, S. K. Chen, S. J. Lin, J. Y. Gan, T. S. Chin, T. T. Shun, C. H. Tsau, and S. Y. Chang, "Nanostructured high-entropy alloys with multiple principal elements: Novel alloy design concepts and outcomes," *Adv. Eng. Mater.*, vol. 6, no. 5, pp. 299–303, 2004. https://doi.org/10.1002/adem.200300567

[9] B. Cantor, I. T. H. Chang, P. Knight, and A. J. Vincent, "Microstructural development in equiatomic multicomponent alloys," *Mater. Sci. Eng. A*, vol. 375-377, pp. 213–218, 2004. https://doi.org/10.1016/j.msea.2003.10.257

[10] Y. J. Zhou, Y. Zhang, Y. L. Wang, and G. L. Chen, "Solid solution alloys of Al Co Cr Fe Ni Ti_x with excellent room-temperature mechanical properties," *Appl. Phys. Lett.*, vol. 90, no. 18, p. 181904, 2007. https://doi.org/10.1063/1.2734517

[11] P. Edalati, A. Mohammadi, M. Ketabchi *et al.*, "Ultrahigh hardness in nanostructured dual-phase HEA AlCrFeCoNiNb developed by high-pressure torsion," *J. Alloys Compd.*, vol. 884, p. 161101, 2021. https://www.sciencedirect.com/science/article/pii/S0925838821002960

[12] X. Wang, Z. Xing, J. Hou, W. He, and K. Liu, "Effect of adding ceramic powder on the microstructure, wear and corrosion resistance of NiCrBSi/WC coating," *J. Mater. Res. Technol.*, vol. 15, pp. 4010–4020, 2021. https://doi.org/10.1016/j.jmrt.2021.10.020

[13] G. U. Sheng and C. T. Liu, "Phase stability in high entropy alloys: Formation of solid-solution phase or amorphous phase," *Prog. Nat. Sci. Mater. Int.*, vol. 21, no. 6, pp. 433–446, 2011. https://doi.org/10.1016/S1002-0071(12)60080-X

[14] T. K. Chen, T. T. Shun, J. W. Yeh, and M. S. Wong, "Nanostructured nitride films of multi-element HEAs by reactive DC sputtering," *Surf. Coat. Technol.*, vol. 188-189, pp. 193–200, 2004. https://doi.org/10.1016/j.surfcoat.2004.08.023

[15] B. S. Murty, J. W. Yeh, S. Ranganathan, and P. P. Bhattacharjee, *High-Entropy Alloys*. Elsevier, 2019.

[16] X. Xian, Z. Zhong, B. Zhang, K. Song, C. Chen, S. Wang, J. Cheng, and Y. Wu, "A high-entropy $\mathrm{V}_{35}\mathrm{Ti}_{35}\mathrm{Fe}_{15}\mathrm{Cr}_{10}\mathrm{Zr}_5$ alloy with excellent high-temperature strength," *Mater. Des.*, vol. 121, pp. 229–236, 2017. https://doi.org/10.1016/j.matdes.2017.02.029

[17] Y. Zhang, Y. J. Zhou, J. P. Lin, G. L. Chen, and P. K. Liaw, "Solid-solution phase formation rules for multi-component alloys," *Adv. Eng. Mater.*, vol. 10, no. 6, pp. 534–538, 2008. https://doi.org/10.1002/adem.200700240

[18] J. Gao and R. Li, "New progress in the research of high-entropy alloys," *J. Funct. Mater.*, vol. 2008, no. 7, pp. 1059–1061, 2008.

[19] A. Takeuchi and A. Inoue, "Classification of bulk metallic glasses by atomic size difference, heat of mixing and period of constituent elements and its application to characterization of the main alloying element," *Mater. Trans.*, vol. 46, no. 12, pp. 2817–2829, 2005. https://doi.org/10.2320/matertrans.46.2817

[20] X. Xian, "Study on the microstructure, strengthening mechanisms, and properties of CrMnFeCoNi high entropy alloys," Ph.D. dissertation, Hefei University of Technology, 2018. https://doi.org/10.27101/d.cnki.ghfgu.2018.000005

[21] Q. Ma, "Preparation and microstructure and property study of laser cladded WC reinforced FeCoNiCr high entropy alloy composite coatings," Ph.D. dissertation, Guangdong University of Technology, 2022. https://doi.org/10.27029/d.cnki.ggdgu.2022.000100

[22] X. Yang and Y. Zhang, "Prediction of high-entropy stabilized solid-solution in multi-component alloys," *Mater. Chem. Phys.*, vol. 132, no. 2-3, pp. 233–238, 2012. https://doi.org/10.1016/j.matchemphys.2011.11.021

[23] S. Guo, Q. Hu, C. Ng, and C. Liu, "More than entropy in HEAs: Forming solid solutions or amorphous phase," *Intermetallics*, vol. 41, pp. 96–103, 2013. https://doi.org/10.1016/j.intermet.2013.05.002

[24] Z. Wang, Y. Huang, Y. Yang, J. Wang, and C. T. Liu, "Atomic-size effect and solid solubility of multicomponent alloys," *Scr. Mater.*, vol. 94, pp. 28–31, 2015. https://doi.org/10.1016/j.scriptamat.2014.09.010

[25] S. Guo, C. Ng, J. Lu, and C. T. Liu, "Effect of valence electron concentration on stability of fcc or bcc phase in high entropy alloys," *J. Appl. Phys.*, vol. 109, no. 10, p. 103505, 2011. https://doi.org/10.1063/1.3587228

[26] Z. Zhang, S. Huang, L. Chen, B. Wang, B. Wen, B. Zhang, and D. Guo, "Ultrahigh hardness on a face-centered cubic metal," *Appl. Surf. Sci.*, vol. 416, pp. 891–900, 2017. https://doi.org/10.1016/j.apsusc.2017.04.223

[27] Y. Zhang, T. T. Zuo, Z. Tang, M. C. Gao, K. A. Dahmen, P. K. Liaw, and Z. P. Lu, "Microstructures and properties of high-entropy alloys," *Prog. Mater. Sci.*, vol. 61, pp. 1–93, 2014. https://doi.org/10.1016/j.pmatsci.2013.10.001

[28] X. Xian, Z. Zhong, B. Zhang, K. Song, C. Chen, S. Wang, J. Cheng, and Y. Wu, "A high-entropy

$V_{35}Ti_{35}Fe_{15}Cr_{10}Zr_5$ alloy with excellent high-temperature strength," *Mater. Des.*, vol. 121, pp. 229–236, 2017. https://doi.org/10.1016/j.matdes.2017.02.029

[29] P. Sharma, V. K. Dwivedi, and S. P. Dwivedi, "Development of high entropy alloys: A review," *Mater. Today: Proc.*, vol. 43, no. 1, pp. 502–509, 2021. https://doi.org/10.1016/j.matpr.2020.12.023

[30] Y. Zhang, Y. J. Zhou, J. P. Lin, G. L. Chen, and P. K. Liaw, "Solid-solution phase formation rules for multi-component alloys," *Adv. Eng. Mater.*, vol. 10, no. 6, pp. 534–538, 2008. https://doi.org/10.1002/adem.200700240

[31] J. Y. He, W. H. Liu, H. Wang, Y. Wu, X. J. Liu, T. G. Nieh, and Z. P. Lu, "Effects of al addition on structural evolution and tensile properties of the FeCoNiCrMn high-entropy alloy system," *Acta Mater.*, vol. 62, no. 1, pp. 105–113, 2014. https://doi.org/10.1016/j.actamat.2013.09.037

[32] S. Liu, M. C. Gao, P. K. Liaw, and Y. Zhang, "Microstructures and mechanical properties of $Al_xCrFeNiTi_{0.25}$ alloys," *J. Alloys Compd.*, vol. 619, pp. 610–615, 2015. https://doi.org/10.1016/j.jallcom.2014.09.073

[33] Z. Sun, M. Zhang, G. Wang, X. Yang, and S. Wang, "Wear and corrosion resistance analysis of $FeCoNiTiAl_x$ high-entropy alloy coatings prepared by laser cladding," *Coatings*, vol. 11, no. 2, 2021. https://doi.org/10.3390/coatings11020155

[34] Y. Li and Y. Shi, "Microhardness, wear resistance, and corrosion resistance of $Al_xCrFeCoNiCu$ HEA coatings on aluminum by laser cladding," *Opt. Laser Technol.*, vol. 134, p. 106632, 2021. https://doi.org/10.1016/j.optlastec.2020.106632

[35] S. Hedya, L. Mohamed, G. Gaber, O. Elkady, H. Megahed, and S. Abolkassem, "Effect of Si/Ti additions on physico-mechanical and chemical properties of FeNiCrCo high entropy alloys manufactured by powder metallurgy technique," *Trans. Nonferrous Met. Soc. China*, vol. 32, no. 8, pp. 2648–2664, 2020. https://doi.org/10.1016/S1003-6326(22)65973-9

[36] W. Hao, R. Sun, W. Niu, X. Li, M. Gu, and R. Zuo, "Microstructure and properties of laser cladded $CoCrFeNiSi_x$ high entropy alloy coatings," *Surf. Technol.*, vol. 50, no. 5, pp. 87–94, 2021.

[37] F. Zhou, Q. Liu, and D. Liang, "Microstructure and properties research of laser cladded $MoFeCrTiWSi_x$ multicomponent alloy coatings," *Rare Met. Mater. Eng.*, vol. 46, no. 12, pp. 3941–3946, 2017.

[38] X. An, Q. Liu, and B. Zheng, "Microstructure and properties of high-entropy alloy MoFeCrTiWAlxSiy coatings prepared by laser cladding," *Infrared Laser Eng.*, vol. 43, no. 04, pp. 1140–1144, 2014.

[39] J. Liu, H. Liu, P. Chen, and J. Hao, "Microstructural characterization and corrosion behaviour of $AlCoCrFeNiTi_x$ HEA coatings fabricated by laser cladding," *Surf. Coat. Technol.*, vol. 361, pp. 63–74, 2019. https://doi.org/10.1016/j.surfcoat.2019.01.044

[40] X. Wang, Q. Liu, Y. Huang, L. Xie, Q. Xu, and T. Zhao, "Effect of Ti content on the microstructure and corrosion resistance of $CoCrFeNiTi_x$ high entropy alloys prepared by laser cladding," *Mater.*, vol. 13, no. 10, p. 2209, 2020. https://doi.org/10.3390/ma13102209

[41] Z. Gu, S. Xi, and C. Sun, "Microstructure and properties of laser cladding and $CoCr_{2.5}FeNi_2Tix$ HEA composite coatings," *J. Alloys Compd.*, vol. 819, p. 152986, 2020. https://doi.org/10.1016/j.jallcom.2019.152986

[42] H. Wu, G. Chen, X. Tang, and S. Shu, "Effect of Cu content on the microstructure and properties of $CoCrFeNiMnAlCu_x$ high entropy alloys," *Nonferrous Met. Eng.*, vol. 12, no. 7, pp. 1–10, 2022.

[43] J. Zhu, J. Meng, and J. Liang, "Microstructure and mechanical properties of multi-principal component $AlCoCrFeNiCu_x$ alloy," *Rare Met.*, vol. 35, pp. 385–389, 2016. https://doi.org/10.1007/s12598-014-0268-5

[44] A. Verma, P. Tarate, A. C. Abhyankar, M. R. Mohape, D. S. Gowtam, V. P. Deshmukh, and T. Shanmugasundaram, "High temperature wear in $CoCrFeNiCu_x$ high entropy alloys: The role of Cu," *Scr. Mater.*, vol. 161, pp. 28–31, 2019. https://doi.org/10.1016/j.scriptamat.2018.10.007

[45] Y. Hsu, W. Chiang, and J. Wu, "Corrosion behavior of $FeCoNiCrCu_x$ HEAs in 3.5% sodium chloride solution," *Mater. Chem. Phys.*, vol. 92, no. 1, pp. 112–117, 2005. https://doi.org/10.1016/j.matchemphys.2005.01.001

[46] J. W. Yeh, S. K. Chen, S. J. Lin, J. Y. Gan, T. S. Chin, T. T. Shun, C. H. Tsau, and S. Y. Chang, "Nanostructured high-entropy alloys with multiple principal elements: Novel alloy design concepts and outcomes," *Adv. Eng. Mater.*, vol. 6, no. 5, pp. 299–303, 2004. https://doi.org/10.1002/adem.200300567

[47] J. Yeh, "Recent progress in high entropy alloys," *Ann. Chim. Sci. Mat.*, vol. 31, pp. 633–648, 2006.

[48] X. Wang and Z. Xing, "Preparation and properties of composite nanoceramic NiCrBSi-TiO_2/WC (Co) coatings," *Coatings*, vol. 10, no. 9, p. 868, 2020. https://doi.org/10.3390/coatings10090868

[49] Y. B. Peng, W. Zhang, T. C. Li, M. Y. Zhang, L. Wang, Y. Song, S. H. Hu, and Y. Hu, "Microstructures and mechanical properties of FeCoCrNi high entropy alloy/WC reinforcing particles composite coatings prepared by laser cladding and plasma cladding," *Int. J. Refract. Met. Hard Mater.*, vol. 84, p. 105044, 2019. https://doi.org/10.1016/j.ijrmhm.2019.105044

[50] Z. Huang, C. Zhang, Q. Tang, P. Dai, and B. Wu, "The effect of wc particles on the microstructure and hardness of laser cladded FeCoCrNiCu high entropy alloy coatings," *China Surf. Eng.*, vol. 26, no. 1, pp. 13–19, 2013.

[51] Q. Zhang, H. Rao, Z. Shen, Z. Huang, and P. Dai, "Effect of WC particles on the microstructure and wear resistance of laser cladded FeCoCrNiB high entropy alloy coatings," *Hot Work. Technol.*, vol. 43, no. 18, pp. 147–150, 2014. https://doi.org/10.14158/j.cnki.1001-3814.2014.18.038

[52] Y. Cai, L. Zhu, Y. Cui, M. Shan, H. Li, Y. Xin, and J. Han, "Fracture and wear mechanisms of FeMnCrNiCo+ x (TiC) composite high-entropy alloy cladding layers," *Appl. Surf. Sci.*, vol. 543, p. 148794, 2020. https://doi.org/10.1016/j.apsusc.2020.148794

[53] Y. Guo, C. Li, M. Zeng, J. Wang, P. Deng, and Y. Wang, "In-situ TiC reinforced $\mathrm{CoCrCuFeNiSi}_{0.2}$ high-entropy alloy coatings designed for enhanced wear performance by laser cladding," *Mater. Chem. Phys.*, vol. 242, p. 122522, 2019. https://doi.org/10.1016/j.matchemphys.2019.122522

[54] X. Li, Y. Feng, B. Liu, D. Yi, X. Yang, W. Zhang, G. Chen, Y. Liu, and P. Bai, "Influence of NbC particles on microstructure and mechanical properties of AlCoCrFeNi HEA coatings prepared by laser cladding," *J. Alloys Compd.*, vol. 788, pp. 485–494, 2019. https://doi.org/10.1016/j.jallcom.2019.02.223

[55] Y. Feng, X. Li, B. Liu, D. Yi, X. Wang, S. Wang, and P. Bai, "Influence of SiC particles on the microstructure and mechanical properties of AlCoCrFeNi high entropy alloy coatings," *Hot Work. Technol.*, vol. 48, no. 8, pp. 160–163, 2019. https://doi.org/10.14158/j.cnki.1001-3814.2019.08.040

[56] Y. Feng, "The influence of ceramic phases on the microstructure and properties of laser cladded AlCoCrFeNi high entropy alloys," Ph.D. dissertation, North University of China, 2019.